Comprehensive Study of Steam Reforming of Methane in Membrane Reactors

Özgün Yücel[1]
Department of Chemical Engineering,
Gebze Technical University,
Gebze, Kocaeli 41400, Turkey
e-mail: yozgun@gtu.edu.tr

Mehmet Alaittin Hastaoglu
Department of Chemical Engineering,
Gebze Technical University,
Gebze, Kocaeli 41400, Turkey
e-mail: hastaoglu@gtu.edu.tr

A 2D model and heat transfer mechanism are proposed to analyze and study oxidative steam reforming of methane (OSRM) in a membrane reactor. The model describes mass and thermal dispersions for gas and solid phases. It also accounts for transport through the membrane. The effects of operating parameters on methane conversion and H_2 yield are analyzed. The parameters considered are the bed temperature (800–1100 K), molar oxygen-to-carbon ratio (0.0–0.5), and steam-to-carbon ratio (1–4). The results show that our model prevents overestimation and provides valuable additional information about temperature and concentration gradients in membrane reactor which is not available in a simple one-dimensional approach. Simulation results show that large temperature and concentration gradients cannot be avoided. The particle properties and the bed diameter have a considerable effect on the extent of gas mixing. Effective gas mixing coefficient also increases with increasing gas and solid velocity. In membrane reactor, simulation results show that mixing which depends on operational and design parameters has a strong effect on the hydrogen conversion. Also, the removal of hydrogen with membranes breaks equilibrium barrier leading to efficient production of hydrogen, reduced reactor size, and tube lengths. The model can be used in real-time simulation of industrial reactors for control and optimization purposes. [DOI: 10.1115/1.4032733]

Keywords: simulation, methane reforming, hydrogen production, membrane reactors

1 Introduction

Hydrogen is a clean energy source which can be produced from methane via catalytic reactions. Steam reforming of methane (SRM) is currently a well-established technology and has been the most important industrial process for the production of hydrogen and synthesis gas (syngas, $CO + H_2$) as feedstock for the manufacture of methanol, ammonia, and other valuable chemicals [1]. Reforming reactions take place at high temperatures (1000–1300 K) in the presence of a metal-based catalyst (nickel), converting large amounts of CH_4 to a mixture of H_2 and CO. This requires substantial heat and complicated reactor design [2].

The fuel consumption rate is typically between 30% and 50% of the feed rate. A typical industrial steam reformer may contain 40–400 tubes surrounded by huge external furnaces. Tube diameter may vary from 70 to 160 mm while wall thickness of tubes varies from 10 to 20 mm. Depending on the type of furnace, heated length also varies from 6 to 12 m [3,4]. Long tubes are needed to achieve the associated fuel reforming thermodynamic limit [5]. Also, conventional reformers generally made of expensive alloys are limited by design temperature and creep rupture strength. Slight increase in the reactor wall temperature may result in a serious decline in the expected tube lifetime. This phenomenon is called heat transfer limitation [6]. For this purpose, autothermal reforming (ATR) has gained importance. In ATR, total oxidation and steam reforming are carried out simultaneously where the heat produced in exothermic partial oxidation is used in endothermic steam reforming. Since heat is generated inside the reactor, the system operates autothermally. Thus, H_2 production is higher per kilogram of catalyst in comparison to steam reforming, and the product composition can be controlled by changing $CH_4/O_2/H_2O$ ratios.

Due to endothermic nature of steam reforming, CH_4 conversion and H_2 yield increase with temperature. On the other hand, carbon formation increases with increase in temperature, leading to catalyst deactivation and blockage of the reformer [7]. However, the maximum yield and conversion that can be attained in conventional packed beds are limited owing to the thermodynamic reversibility of the SRM reactions. Membrane technology can be used for H_2 separation to drive the reaction beyond the normal thermodynamic equilibrium for the same temperature, pressure, and steam/methane feed rates. Especially, palladium-based membranes offer a promising method for extracting hydrogen from syngas [8].

The movement of solid particles within a fluidized bed reactor limits the net amount of carbon formation by recirculating the catalyst to the oxygen-rich zones of the bed, and the interparticle mass transfer resistance is negligible in the high mass flow rate conditions [9]. The temperature uniformity offered by a fast fluidized bed is also advantageous because it reduces thermal stresses on the membrane material. In a fast fluidized bed membrane reactor, methane conversion and the total removal rate of hydrogen increase with reactor pressure, contrary to the conventional fixed bed reactors. At higher pressures, water–gas shift reaction may consume all CO and produce CO_2 and H_2. However, due to production cost and use of hydrogen fuel cells for versatile applications, processes with cheaper initial cost had to be developed. For efficient hydrogen production, conventional fixed bed reformers should be modified in four major areas:

- improve the catalyst to overcome deactivation and diffusion limitation
- separate the hydrogen using membrane technology
- change the reactor operation from packed bed to fluidized bed
- operate reactor autothermally (with oxygen or air)

In this work, OSRM in a fast fluidized bed membrane reactor is studied for overcoming thermodynamic equilibrium limits leading to higher efficiency in H_2 production. A 2D mathematical model

[1]Corresponding author.

Contributed by the Advanced Energy Systems Division of ASME for publication in the Journal of Energy Resources Technology. Manuscript received September 30, 2015; final manuscript received January 29, 2016; published online March 1, 2016. Editor: Hameed Metghalchi.

Table 1 Reactions and rate equations

Reaction	Heat of reaction	Kinetic rate equation	References
$CH_4 + H_2O \rightarrow CO + 3H_2$	$\Delta H^{\circ}_{298} = 206.2$	$r_1 = k_1 \left(\frac{P_{CH_4} P_{H_2O}}{P^{2.5}_{H_2}} - \frac{P_{CO} P^{0.5}_{H_2}}{K_1} \right) / \mathrm{DEN}^2$	[7]
$CO + H_2O \rightarrow CO_2 + H_2$	$\Delta H^{\circ}_{298} = -41.2$	$r_2 = k_2 \left(\frac{P_{CO} P_{H_2O}}{P_{H_2}} - \frac{P_{CO_2}}{K_2} \right) / \mathrm{DEN}^2$	[7]
$CH_4 + 2H_2O \rightarrow CO_2 + 4H_2$	$\Delta H^{\circ}_{298} = 165$	$r_3 = k_3 \left(\frac{P_{CH_4} P^2_{H_2O}}{P^{3.5}_{H_2}} - \frac{P_{CO_2} P^{0.5}_{H_2}}{K_2 K_1} \right) / \mathrm{DEN}^2$	[7]
$CH_4 + 2O_2 \rightarrow CO_2 + 2H_2O$	$\Delta H^{\circ}_{298} = -802.7$	$r_4 = k_4 P_{CH_4} P_{O_2}$	[8]
$CH_4 + CO_2 \rightarrow 2CO + 2H_2$	$\Delta H^{\circ}_{298} = 246.9$	$r_5 = k_5 P_{CH_4} P_{CO_2} \left(1 - \frac{P^2_{CO} P^2_{H_2}}{K_5 P_{CH_4} P_{CO_2}} \right)$	[8]

Note: $\mathrm{DEN} = 1 + K_{CO} P_{CO} + K_{H_2} P_{H_2} + K_{CH_4} P_{CH_4} + K_{H_2O} P_{H_2O} / P_{H_2}$.

Table 2 Arrhenius kinetic parameters and reaction equilibrium constants

Reaction, j	Equilibrium constant	Pre-exponential factor	Activation energy (kJ/mol)
1	$e^{-26830/T+30.114}$	1.17×10^{15}	240.1
2	$e^{4400/T-4.036}$	5.43×10^{5}	67.13
3		2.83×10^{14}	243.9
4		3.96×10^{7}	166.0
5	$e^{-30782/T+42.97}$	8.71×10^{-2}	23.7

for reactors is developed to investigate the effects of operating parameters on methane conversion and H_2 yield in OSRM. The parameters considered are the bed temperature (800–1100 K), molar oxygen-to-carbon ratio (O/C = 0.0–0.5), and steam-to-carbon ratio (S/C = 1–4).

2 Mathematical Model

A working mathematical model that could aid to further understand the performance of the reactor is developed. The computational model is developed to investigate the performance of fast fluidized bed membrane reactors to increase efficiency of hydrogen production. The reactor is considered as pseudo-homogeneous to simplify the problem of accounting for the two phases in the flow. This essentially means that the catalyst mass is assumed to be uniformly distributed throughout the fluidized bed. A simplified two-dimensional diffusion-reaction model is chosen to take into account the radial heat and mass dispersion due to gas flow through membrane. It also includes the coupling of steam reforming and oxidative reforming of methane. Model validation has been performed against experimental reaction data. The following assumptions are made:

(i) Gases are incompressible and obey the ideal gas law.
(ii) The slip between the solid and gas phases is negligible.
(iii) Solid fraction is constant in axial and radial directions.
(iv) The membrane permeates hydrogen only.
(v) Permeating gases are in plug flow.
(vi) Due to the large mass flow ratio of catalyst to gas, catalyst deactivation is negligible.
(vii) The internal diffusional resistance of the catalyst particles is negligible.
(viii) Kinetic and pressure terms in the energy equation are negligible.
(ix) The effect of viscous heating is negligible.
(x) The heat capacities of the components are constant.
(xi) Thermal radiation is not considered.

2.1 Reaction Kinetic Model. Xu and Froment [10] developed rate expressions based on the Langmuir–Hinshelwood–Hougen–Watson approach after experiments done at temperatures above 500 °C. This model considered a 13-step reaction scheme of which three are rate determining. Jin et al. [11] assumed that the partial oxidation of methane to synthesis gas does not occur as an elementary reaction step; it contains steam reforming, dry reforming of CH_4, and total oxidation of CH_4. This reaction mechanism is widely accepted. The model can be operable under steam reforming and ATR conditions. Thus, the reactions considered in the model are composed of SRM from Xu and Froment [10] and partial oxidation of methane from Jin et al. [11]. Table 1 summarizes the main reactions and assumed kinetics.

Table 3 van't Hoff parameters for species adsorption

Reaction rate constant	Pre-exponential factor	Adsorption enthalpy (kJ/mol)
K_{CH_4} (bar^{-1})	6.65×10^{-4}	−38.28
K_{CO} (bar^{-1})	8.23×10^{-5}	−70.65
K_{H_2O} (bar)	1.77×10^{5}	88.68
K_{H_2} (bar^{-1})	6.12×10^{-11}	−82.90

Here, r_j is the rate of reaction, k_j is the reaction rate constant, K_j is the equilibrium constant of reaction j (j = 1–6), K_i is the adsorption constant, and P_i is the partial pressure of species i ($i = CH_4$, H_2O, etc). The partial pressure of each component at any point in the reactor can be calculated as $P_i = P_t C_i / C_t$. The kinetic data are shown in Tables 2 and 3 as $k_j = k_{oj} e^{-E_j/RT}$ and $K_i = K_{oi} e^{-\Delta H_i/RT}$.

2.2 Governing Equations. The model developed is typically comprised of conservation equations in the gas and the solid phases. To account for the local mixing, membrane effects, and nonideal flow characteristics, 2D reactor model is found to be more appropriate than 1D. Part of the model equations which can also be used for fixed bed reactors is given below. Transport coefficients and thermophysical properties are continuously evaluated using well-established correlations and methods. The set of equations are solved via finite-difference techniques, and a small amount of the results is presented below.

Material and energy balances in gas phase are given by

$$\varepsilon\frac{\partial C_i}{\partial t}=D_i\left(\frac{\partial^2 C_i}{\partial r^2}+\frac{1}{r}\frac{\partial C_i}{\partial r}+\frac{\partial^2 C_i}{\partial z^2}\right)-u\frac{\partial C_i}{\partial z}+h_{D_i}S_{\text{cat}}(C_{si}-C_i) \tag{1}$$

$$\varepsilon\rho_g c_{pg}\frac{\partial T_g}{\partial t}=-u\rho_g c_{pg}\frac{\partial T_g}{\partial z}+S_h h_{pg}(T-T_g) \tag{2}$$

Material and energy balances in solid phase

$$\rho_b c_{pp}\frac{\partial T}{\partial t}=k_{pp}\left(\frac{\partial^2 T}{\partial r^2}+\frac{1}{r}\frac{\partial T}{\partial r}+\frac{\partial^2 T}{\partial z^2}\right)-u\rho_p c_{pp}\frac{\partial T}{\partial z}+S_h h_{pg}(T_g-T)+\rho_p\sum_{j=1}^{4}(-\Delta H_j\eta_j R_j) \tag{3}$$

$$\rho_{\text{cat}}r_i=h_{D_i}S_{\text{cat}}(C_{si}-C_i) \tag{4}$$

Momentum balance [12]

$$\frac{\partial P}{\partial z}=-\frac{150\mu_g(1-\varepsilon_b)^2}{d_p^2\varepsilon_b^3}u-\frac{1.75(1-\varepsilon_b)\rho_g}{d_p\varepsilon_b^3}u^2 \tag{5}$$

Variation of superficial velocity

$$u=\frac{RT}{PA}\sum_{i=1}^{N}F_i \tag{6}$$

For dense palladium membrane, the rate of hydrogen permeation is [13]

$$J_{\text{H}_2}=-\frac{7.21\ \ 10^{-2}}{\delta_{\text{H}_2}}\ \exp\left(\frac{-15700}{RT}\right)\left(\sqrt{\rho_{\text{H}_2,r}}-\sqrt{\rho_{\text{H}_2,p}}\right) \tag{7}$$

The equations given above are solved for a reactor of 2 m length and 8 cm diameter. H_2 membranes are placed at the exterior reactor surfaces (see Fig. 1). Inlet gas flow rates of methane, water steam, carbon monoxide, and hydrogen are, respectively, 3, 12, 0.5, and 0.5 kmol/hr. But simulations are made for different steam–carbon and oxygen–carbon ratios at various temperatures and pressures. The catalyst and gas temperatures are initially equal to the feed temperature at the start-up conditions. The initial and boundary conditions are set as follows:

$$\text{at } t=0\begin{cases}T=T_0\\ C_s=C_{s0}\end{cases}\text{at } z=0 \text{ and}$$

$$t>0\begin{cases}T_g=T_g^{\text{in}}\\ C_i=C_i^{\text{in}}\\ P=P^{\text{in}}\\ u_{\text{in}}=\dfrac{RT_{\text{in}}}{P_{\text{in}}}\displaystyle\sum_{i=1}^{N}F_{i_{\text{in}}}\end{cases}\quad\text{at } z=L \text{ and } t>0\begin{cases}\dfrac{\partial C_i}{\partial z}=0\\ \dfrac{\partial T_g}{\partial z}=0\end{cases} \tag{8}$$

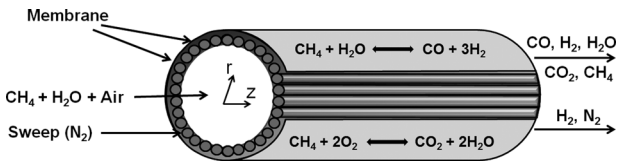

Fig. 1 A schematic representation of the reformer

$$\text{at } r=0\begin{cases}\dfrac{\partial C_i}{\partial r}=0\\ \dfrac{\partial T_g}{\partial r}=0\end{cases}\qquad\text{at } r=R\begin{cases}\dfrac{\partial C_{gi}}{\partial r}=0 \quad\text{except for hydrogen}\\ D_{\text{H}_2}\dfrac{\partial C_{\text{H}_2}}{\partial r}=J_{\text{H}_2} \quad\text{for hydrogen}\\ (k_{pp}+k_g)\dfrac{\partial T}{\partial r}=\propto(T-T_a)\end{cases} \tag{9}$$

2.3 Heat and Mass Transfer Coefficients. A number of mechanistic models have been proposed to describe the particle convective component and explain the nature of heat transfer at the walls. These models can be classified into three groups: continuous film models, cluster renewal models, and single particle models [14]. Congregation of solid particles into clusters is a major characteristic of most circulating fluidized beds.

The heat transfer model and its parameters especially are selected to apply to the fast fluidized regime but some aspects of the model are appropriate for other fluidization regimes. Heat transfer model for fluidized bed involves three mechanisms: (1) convection between gas and particles, (2) conduction between particles, and (3) both convection and conduction between gas–solid suspension and reactor walls.

In homogeneous gas–particle systems, Rowe et al. [15] suggested an equation for heat transfer coefficient between gas and particles as

$$h_{pg}=2\varepsilon_c\frac{k_g}{d_p}+0.69\frac{k_g}{d_p}\left(\frac{u_s d_p p_g}{\varepsilon\mu_g}\right)^{1/2}\left(\frac{c_{pg}\mu_g}{k_g}\right)^{1/3} \tag{10}$$

Mass transfer coefficient between particle and gas

$$h_D=2\varepsilon_c\frac{D}{d_p}+0.69\frac{D}{d_p}\left(\frac{u_s d_p p_f}{\varepsilon\mu_g}\right)^{1/2}\left(\frac{c_{pg}\mu_g}{k_g}\right)^{1/3} \tag{11}$$

The thermal conductivity of gas and particles in a homogeneous system is approximated by Hastaoglu et al. [16], and the effective thermal conductivity is

$$k_{pp}=(1-\varepsilon)^2k_p+\varepsilon^2k_g \tag{12}$$

Overall heat transfer coefficient α through the reformer wall is determined from

$$\frac{1}{\alpha}=\frac{1}{h_{wi}}+\frac{b}{k}+\frac{1}{h_{w0}} \tag{13}$$

The descent of these clusters takes place primarily in the gas–solid wall layer adjacent to the reactor wall. So, the overall heat transfer coefficient may be expressed as a function of time-average fraction of the wall covered by clusters as [17]

$$f=1-\exp\left[-4300(1-\varepsilon)^{1.39}\left(\frac{d_p}{L}\right)^{0.22}\right] \tag{14}$$

Heat transfer coefficient from a cluster may be obtained by adding the contact resistance and the transient conduction resistance to a cluster of particles calculated independently. The combination of cluster convection, gas-gap conduction, and the dispersed phase convection heat transfer coefficients is given below

$$h_{wi}=f\left(\frac{1}{h_{cw}}+\frac{1}{h_{ce}}\right)^{-1}+(1-f)h_d \tag{15}$$

$$h_{wi} = f\left(\frac{\delta_w d_p}{k_g} + \sqrt{\frac{\pi\tau}{k_{pp}c_{pp}\rho_p(1-\varepsilon)}}\right)^{-1} + (1-f)0.023\frac{k_g}{d_p}\mathrm{Re}_D^{0.8}\mathrm{Pr}^{0.3} \quad (16)$$

Free convection heat transfer coefficient outside of the reactor walls is determined from [18]

$$h_{w0} = \frac{k_a}{d_0}\left\{0.6 + \frac{0.387\,\mathrm{Ra}^{1/6}}{\left[1+(0.559/\mathrm{Pr})^{9/16}\right]^{8/27}}\right\}^2 \quad (17)$$

The governing equations with initial and boundary conditions combined with the heat and mass transfer coefficients are solved for the temperature and gas concentrations along and across the reactor using a finite-difference method. Since the partial pressure of hydrogen is in the denominator, it is not possible to calculate the rates of steam reforming reactions from Xu and Froment [10], when there is no hydrogen in the feed. To overcome this problem, a small amount of hydrogen is always considered to be present in the feed for the purpose of simulation which would have little impact on the overall performance of the reactor simulation. Table 4 shows the operational parameters simulated.

The set of equations given above were discretized with explicit finite-difference method and solved via explicit Euler integrator with variable time step (max 1×10^{-5}). Mesh grid size is 20 mm in radial and 20.2 mm in axial direction. Computational grid has 5 radial and 100 axial points with a total of 500 points. Also, we have additional one-dimensional axial 100 points for membrane side in order to integrate the collected hydrogen. However, the number of grid points can easily be changed. Convergence criteria were 1×10^{-5} in terms of relative error. All the equations were solved simultaneously, with other auxiliary equations.

2.4 Model Verification. The use of computational fluid dynamics (CFD) software known as FLUENT for the purpose of modeling transport phenomena and heat transfer within a given geometry has become a common approach to solve transport problems. To represent the geometry of the reformer, a two-dimensional, axisymmetric flow is chosen. A number of assumptions are made to simplify the CFD model. The temperature and porosity are assumed constant along the reactor and the membrane is ignored. For verification of the model, the results of the model simulations are compared with solutions obtained from FLUENT and a model reported by Chen et al. [19], which are for the same feed ratios and bed configurations at isothermal conditions.

The comparison of the model with the Chen model and CFD model is shown in Fig. 2, where a consistency between all models for higher bed temperatures is apparent. On the other hand, for lower temperatures at which reaction rate is low, the direction of reaction deviates and kinetics becomes highly nonlinear. As a result, a deviation of the model from FLUENT-based model can be observed clearly. The difference between the results of FLUENT and developed models stems from the fact that a user-defined function is developed and added to FLUENT for the calculation of reaction kinetics. So, FLUENT model is based on the concept of ideal mixing, especially at lower temperatures, to prevent local uniformities of temperature and concentrations in the reactor. Thus, it is concluded that FLUENT overestimated the results at lower temperatures that are close to reaction equilibrium. However, the discrepancy between three models is small. It is noted that other two models have well mixing characteristic, so gas concentrations in each region are equal at all radii. This work shows that there are always concentration gradients at all radii. This is the reason why the model underestimates hydrogen yield compared to other models. Also, in fluidized bed chemical reactors, back-mixing of axial gas can strongly decrease the conversion and selectivity.

3 Results and Discussion

In this section, the effects of membrane on composition of gases, results of H_2 yield and CH_4 conversion are exhibited. The feed temperature, oxygen-to-carbon ratio, and steam-to-carbon ratio are varied. The methane conversion is defined as the total moles of process methane converted per mole of process methane fed, and the total hydrogen yield is defined as the total moles of hydrogen produced per mole of process methane fed.

3.1 Effect of Feed Temperature. In order to investigate the effects of membrane at various temperatures, the model is simulated at several isothermal conditions (800, 900, 1000, and 1100 K). But bed temperature cannot be changed alone by keeping all other variables constant. If superficial velocity is fixed, molar flow rate of methane will change, and thus, contact time will deviate. In this work, while molar flow rates are fixed, superficial velocity varies due to gas law. The range of bed temperatures in the analysis is 800–1100 K, which would vary superficial velocity a little. But this change in superficial velocity affects the reactor performance to some extent.

Because of endothermic nature of steam reforming, methane conversion and hydrogen yield increased with temperature. But maximum temperature studied is 1100 K at this work. At this temperature, 97% of methane can be converted without membrane. Also, the equilibrium constant of water–gas shift reaction is 1 at

Table 4 Reactor parameters and operating conditions used in the model simulations

Reformer tube length (m)	2
Inside diameter of reformer tube (m)	0.08
Outside diameter of the reformer tube (m)	0.1
Solid fraction	0.1
Particle density (kg/m^3)	2200
Particle diameter (m)	0.004
Temperature with steps of 100 (K)	800–1100
Pressure with steps of 5 atm (kPa)	506.5–1519.5
Gas velocity (m/s)	1.7
Steam-to-carbon ratio (S/C, mol/mol)	3
Diameter of hydrogen permeable membrane tubes (m)	0.0098
Thickness of palladium hydrogen membranes (μm)	20
Number of palladium hydrogen membranes	20
Pressure on the membrane side (kPa)	101
Sweep gas flow rate, N_2 (mol/s)	0.2

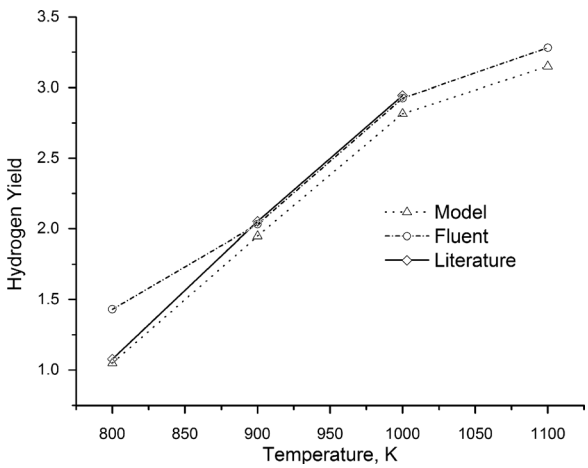

Fig. 2 Verification of the model

around 1100 K. Water–gas shift reaction describes the reaction of CO and water vapor to form CO_2 and H_2 and determines the equilibrium point of the reformer. The equilibrium constant of water–gas shift reaction decreases with temperature. Beyond 1100 K, it will be reversed. So, the maximum CH_4 conversion and H_2 yield can be achieved at this temperature. As shown in Fig. 3, CH_4 conversion increases with temperature and maximum CH_4 conversion can be achieved at 1100 K.

The hydrogen permeability of the pure palladium membrane is tested at various temperatures in literature. But there is no work about selectivity performance of pure palladium membranes over 1100 K. However, some publications indicate that carbon and oxygen solubility in palladium increases with temperature which is close to the hydrogen solubility. We have no data about the stability and performance of palladium membranes for their effectiveness in hydrogen separation beyond this temperature. Figure 3 also shows that CO/CO_2 ratio increases with temperature. The direction of the water gas shift reaction changed from CO_2 to CO production when the temperature is increased. Dashed H_2 line in Fig. 3(*b*) shows collected hydrogen at membrane side.

Figure 4 demonstrates temperature effect on H_2 yield and CH_4 conversion along the reactor with and without membrane. The isothermal operation mode represents an idealized situation but temperature effect on reactor performance can be seen clearly. The dashed lines in figures show the cases with membrane. More hydrogen is extracted via membrane, and thus, the reforming reactions shift to give more products including hydrogen [20]. As may be seen from these figures, hydrogen membrane has a pronounced effect on methane conversion and total yield of hydrogen. Another positive effect of temperature on productivity is that hydrogen membrane permeability increases with increasing temperature. Because of this, the reaction shifts to the product side. As seen in Fig. 4, the variations of concentrations of components are sharp only at the entrance of the reactor (about 4%), after that, they vary more slowly. Composition of the gas stream reaches near equilibrium at the end of the bed.

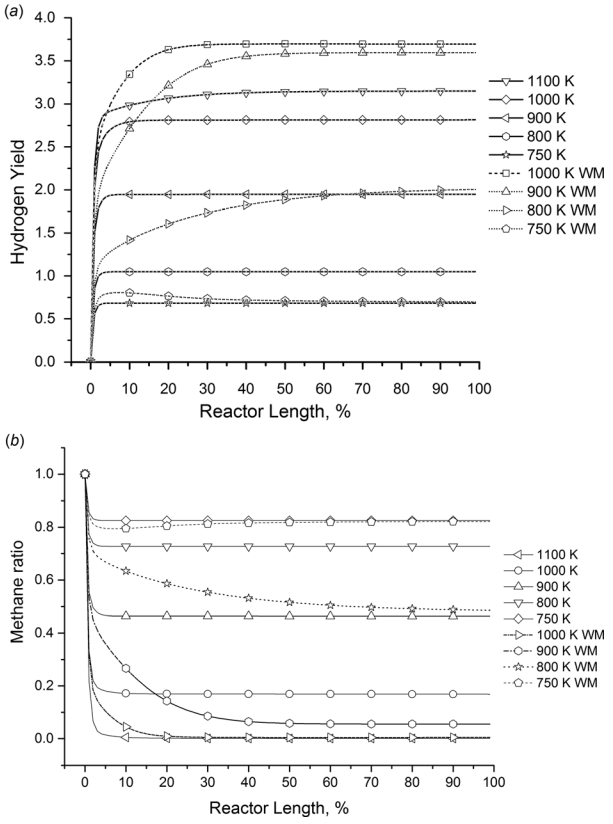

Fig. 4 (*a*) Hydrogen yield and (*b*) methane conversion for the cases with membranes and without for isothermal simulation

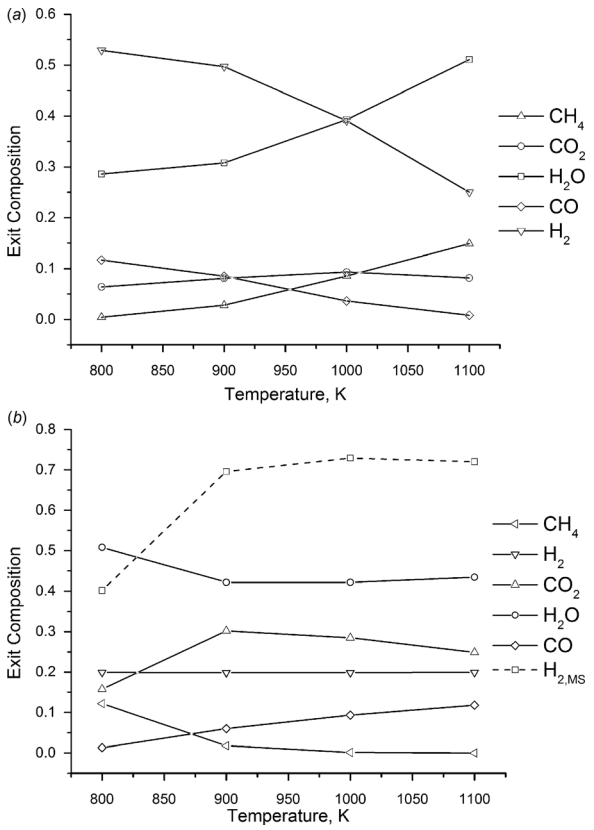

Fig. 3 Exit composition versus temperature: (*a*) without membrane and (*b*) with membrane. $H_{2,MS}$ is the membrane side hydrogen.

It can be seen in Fig. 5(*a*) that the reactor temperature decreases as the conversion rate increases. Consequently, the reactor temperature profile becomes unfavorable. Figure 5(*b*) shows that H_2 yield decreases compared to isothermal case. This is expected and can be explained by an increase in the endothermic steam methane reforming. If steam reforming increases, it can reduce the temperature and decrease hydrogen yield and reaction rates. As discussed in the isothermal simulations above, the removal of hydrogen with membranes breaks the thermodynamic equilibrium barrier. But from the point of catalyst stability, these large temperature gradients are undesirable.

Adiabatic reactor performance in terms of H_2 yield in the exhaust is comparable to the isothermal operation mode, because H_2 permeation is comparable in these cases. Nevertheless, the simulation results show that large temperature gradients cannot be avoided, not even with an infinitely high sweep gas rate. To avoid large temperature gradients over the membrane, the membrane should not be placed at sections close to the reactor inlet.

Without H_2 membranes, the total yield H_2 decreases as the reaction pressure increases due to the increase of number of molecules in SRM. But when membranes are used, total yield of hydrogen at high pressure is higher than cases at low reaction pressure, as seen in Fig. 6.

3.2 Effect of Oxygen-to-Carbon and Steam-to-Carbon Ratios. By introducing oxygen to the reactant feed with methane, the large axial temperature gradients can be minimized. The oxygen feed will eventually lead to (hydrogen or methane) combustion and, thus, the temperature increases. Also, significantly

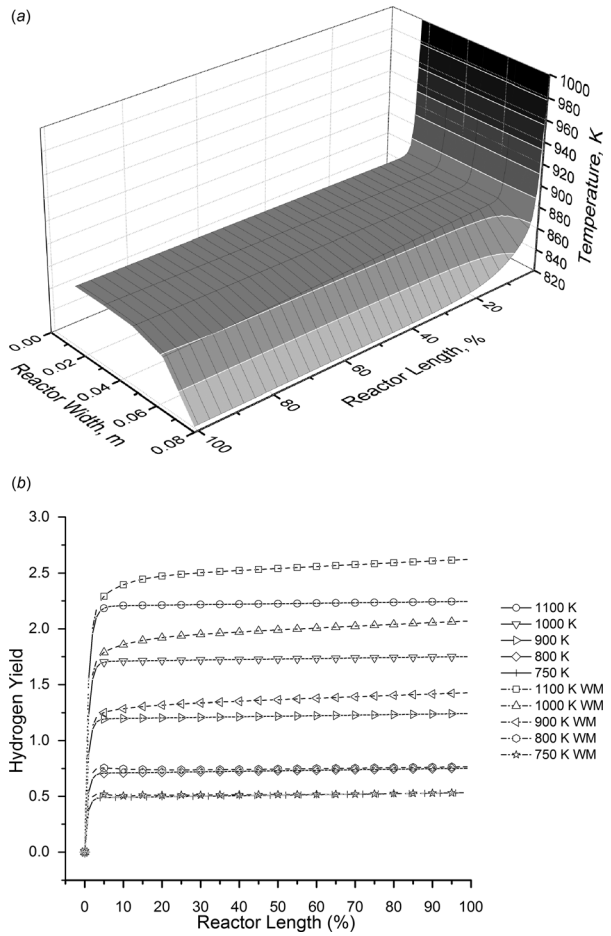

Fig. 5 (*a*) Temperature profile for the case with membrane for adiabatic simulation at 1000 K and (*b*) hydrogen yield for the cases with and without membranes for adiabatic simulations

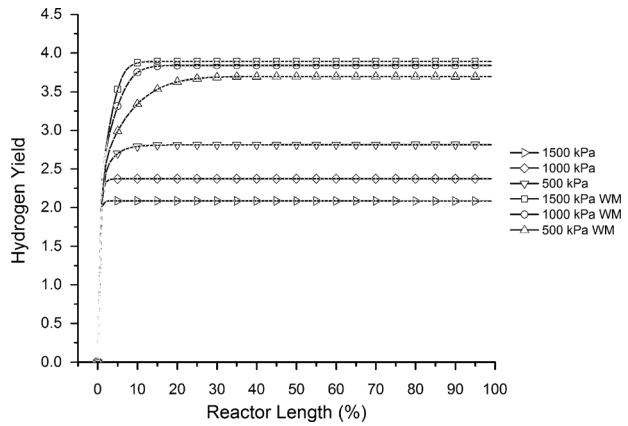

Fig. 6 Hydrogen yield at different reaction pressures for the cases with and without membranes for isothermal simulation

higher average reactor temperature has consequences for overall CH_4 conversion and H_2 production. This is because of higher membrane permeability at higher temperatures. Obviously, when the membrane permeability is increased, the reactor performance is strongly enhanced.

Effect of feed ratio on the product gas distribution is analyzed by changing only the oxygen amount and steam-to-carbon (S/C) ratios while keeping other parameters the same. In Fig. 7, each

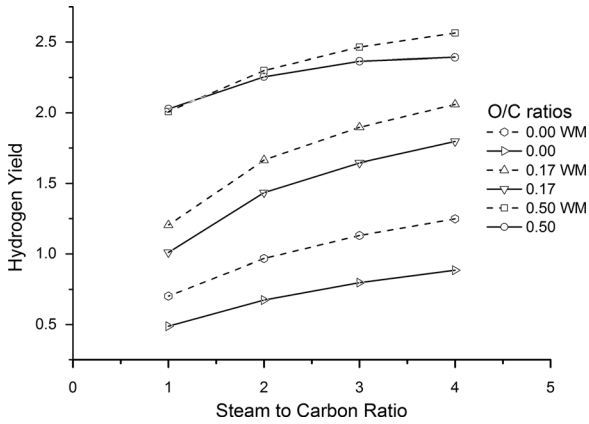

Fig. 7 Fuel conversion efficiency for the cases with and without membranes at 900 K

curve represents the change in H_2 yield with steam-to-carbon ratio for constant oxygen feed ratio. As can be seen, increasing O/C over a certain extent (from 0 to 0.17 then 0.5) affects positively the H_2 output for all S/C ratios selected since the temperature profile is more favorable, although more fuel is consumed in oxidation reactions. Increasing S/C under isothermal/adiabatic condition at constant feed temperature at 900 K and O/C for each run increases the total yield of H_2. This is because an increase in S/C shifts the equilibrium to higher conversion.

3.3 Effect of Mixing. To characterize the gas in the dilute region of a circulating fluidized bed, some authors have defined a gas exchange coefficient between core and annulus, in a similar way to that between the bubble and emulsion phase in bubbling fluidized beds. This type of model assumes that the gas concentrations in each region are equal at all radii, and the wall causes a resistance to the gas diffusion [21]. This work is analyzed using a dispersion model where radial mixing is a significant parameter due to negligible back-mixing compared to the convective flow.

The gas concentrations and radial mixing cannot be measured easily in fast fluidized beds because the mean residence times of the gas in recent fluidized beds are 1 or 2 s. So, there are many correlations for the prediction of the radial gas diffusion coefficient in the literature as a function of operating conditions (external solid flux, air velocity, etc.) and the characteristics of the riser [21–25]. Figure 8 shows the effect of radial flow dispersion coefficient on hydrogen yield.

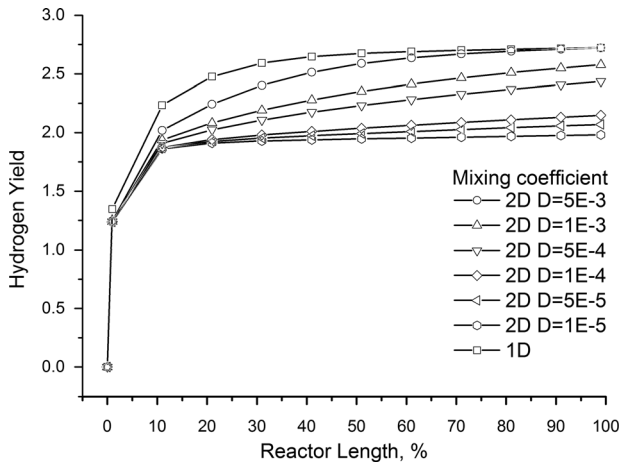

Fig. 8 Effect of radial flow dispersion on hydrogen yield for the cases with membranes

Membrane permeability leads to complete removal of all H_2 produced at total conversion of CH_4. High flux membranes lead to more pronounced radial concentration profiles, and radial mixing determines the concentration gradient. As shown in Fig. 8, at lower dispersion coefficients, membrane effectiveness decreases reducing the reactor performance, which justifies the use of 2D modeling to prevent overestimation of the total hydrogen removal rate. The concentration polarization decreases by increasing the dispersion coefficient.

4 Conclusions

A two-dimensional heterogeneous reactor model has been successfully developed and validated. The model, based on the reforming kinetics, detailed mass, and energy balances, predicts gas yields and temperature and concentration profiles. The study considers five simultaneous chemical kinetic reactions and seven species. The explicit finite-difference method is used to solve the set of equations. The results are comparable to other models.

It is shown that removal of hydrogen with membranes breaks equilibrium barrier leading to efficient production of hydrogen, reduced reactor size, and tube lengths. However, it increases undesirable temperature gradients along the reactor, which are detrimental to membrane and catalyst stability.

The maximum conversion and yield can be achieved at 1100 K, because the overall reaction is exothermic below this temperature and endothermic above it. Increasing the oxygen over a certain extent positively affects the H_2 output for all S/C ratios selected since temperature profile is more favorable although more fuel is being consumed in the oxidation reactions.

The performance of the membrane-reformer improves greatly by including the mixing effects. Thus, 2D modeling is fairly justified. Additionally, the present model is clearer and easier to apply in comparison to other 2D models.

Finally, the model developed can be used for membrane-reactor design for similar systems. It can serve in real-time-on-line simulation of industrial reactors for control and optimization purposes.

Nomenclature

A = reactor cross-sectional area (m^2)
b = wall thickness (m)
C_i, Cs_i = concentration and its surface value (mol/m^3)
c_p = heat capacity (J/kg K)
d = reactor diameter (m)
D = hydraulic diameter of bed (m)
D_i = gas diffusivity of species i (m^2/s)
d_p = catalyst pellet diameter (m)
f = time-average fraction of the wall covered
F = gas flow rate (kmol/s)
h = convective heat transfer coefficient (W/m^2 K)
h_D = convective mass transfer coefficient (m/hr)
J = membrane permeation flux (kmol/hr m^2)
k = thermal conductivity (W/m K)
L = reactor length (m)
P, P_i = total and partial pressures (bar)
Pr = Prandtl number
r, z = cylindrical coordinates
R = gas constant (kJ/kmol K)
R_j, r = conversion rate (kmol/kg cat·hr)
Ra = Rayleigh number
Re = Reynolds number
S_{cat} = catalyst specific area (m^2/m^3)
S_h = heat transfer area per volume of bed (m^2/m^3)
T = temperature (K)
u = superficial velocity (m/s)
ΔH = heat of reaction (kJ/kmol)

Greek Symbols

α = overall wall heat transfer coefficient ($W/K \cdot m^2$)
δ = thickness of membrane (m)
δ_w = dimensionless effective gas layer at the wall
ε = void fraction
η = stoichiometric coefficient
μ = dynamic viscosity (kg/m s)
ρ = density (kg/m^3)
τ = dimensionless residence time

Subscripts

a = ambient
b = bed
c = cluster
cat = catalyst
ce = effective cluster
cw = gas layer
g = gas
i, j = gas and reaction index
i, o = inner and outer, respectively
p = catalyst particles
pp = effective bed
r, m = reactor and membrane side
t = time
w = wall

References

[1] Balthasar, W., 1984, "Hydrogen Production and Technology: Today, Tomorrow and Beyond," Int. J. Hydrogen Energy, **9**(8), pp. 649–668.
[2] Pugsley, T., and Malcus, S., 1997, "Partial Oxidation of Methane in a Circulating Fluidized-Bed Catalytic Reactor," Ind. Eng. Chem. Res., **36**(11), pp. 4567–4571.
[3] Adris, A. M., Pruden, B. B., Lim, C. J., and Grace, C. J., 1996, "On the Reported Attempts to Radically Improve the Performance of the Steam Methane Reforming Reactor," Can. J. Chem. Eng., **74**(2), pp. 177–186.
[4] Rostrup-Nielsen, J. R., 1984, "Sulfur-Passivated Nickel Catalysts for Carbon-Free Steam Reforming of Methane," J. Catal., **85**(1), pp. 31–43.
[5] Mokheimer, E. A., Ibrar Hussain, M., Ahmed, S., Habib, M. A., and Al-Qutub, A. A., 2014, "On the Modeling of Steam Methane Reforming," ASME J. Energy Resour. Technol., **137**(1), p. 012001.
[6] Rostrup-Nielsen, J. R., 1983, "Catalytic Steam Reforming," *Catalysis: Science and Technology*, J. R. Anderson and M. Boudard, eds., Springer, Berlin, p. 289.
[7] Trimm, D. L., 1997, "Coke Formation and Minimization During Steam Reforming Reactions," Catal. Today, **37**(3), pp. 233–238.
[8] Leyko, A. B., and Gupta, A. K., 2013, "Temperature and Pressure Effects on Hydrogen Separation From Syngas," ASME J. Energy Resour. Technol., **135**(3), p. 034502.
[9] de Deken, J. C., Devos, E. F., and Froment, G. F., 1982, "Steam Reforming of Natural Gas: Intrinsic Kinetics, Diffusional Influences, and Reactor Design," Chem. React. Eng., **16**, pp. 181–197.
[10] Xu, J., and Froment, G. F., 1989, "Methane Steam Reforming, Methanation and Water–Gas Shift—I: Intrinsic Kinetics," AIChE J., **35**(1), pp. 88–96.
[11] Jin, W., Gu, X., Li, S., Huang, P., Xu, N., and Shi, J., 2000, "Experimental and Simulation Study on a Catalyst Packed Tubular Dense Membrane Reactor for Partial Oxidation of Methane to Syngas," Chem. Eng. Sci., **55**(14), pp. 2617–2625.
[12] Ergun, S., 1952, "Fluid Flow Through Packed Columns," Chem. Eng. Prog., **48**, pp. 89–94.
[13] Shu, J., Grandjean, B. P. A., and Kaliaguine, S., 1994, "Methane Steam Reforming in Asymmetric Pd– and Pd–Ag/Porous SS Membrane Reactor," Appl. Catal. A, **119**(2), pp. 305–325.
[14] Xie, D., 2001, "Modeling of Heat Transfer in Circulating Fluidized Beds," Ph.D. thesis, The University of British Columbia, Vancouver, BC.
[15] Rowe, P. N., Claxton, K. T., and Lewis, J. B., 1965, "Heat and Mass Transfer From a Single Sphere in an Extensive Flowing Fluid," Trans. Inst. Chem. Eng., **43**, pp. 14–31.
[16] Hastaoglu, M. A., Hilal, N., Abdulkarim, M., and El-Naas, M., 2000, "Transient Multi Gas–Solid Reactions in a Bubbling Fluidized Bed," Can. J. Chem. Eng., **78**(3), pp. 433–441.
[17] Dutta, A., and Basu, B., 2004, "An Improved Cluster-Renewal Model for the Estimation of Heat Transfer Coefficients on the Furnace Walls of Commercial Circulating Fluidized Bed Boilers," ASME J. Heat Transfer, **126**(6), p. 001040.
[18] Chan, S. H., Hoang, D. L., and Ding, O. L., 2005, "Transient Performance of an Autothermal Reformer—A 2-D Modeling Approach," Int. J. Heat Mass Transfer, **48**, pp. 19–20.
[19] Chen, Z., Yan, Y., and Elnashaie, S. S. E. H., 2003, "Novel Circulating Fast Fluidized-Bed Membrane Reformer for Efficient Production of Hydrogen From Steam Reforming of Methane," Chem. Eng. Sci, **58**(19), p. 4335.

[20] Dehkordi, A. M., and Memari, M., 2009, "Compartment Model for Steam Reforming of Methane in a Membrane-Assisted Bubbling Fluidized-Bed Reactor," Int. J. Hydrogen Energy, **34**(3), pp. 1275–1291.
[21] Gayan, P., de Diego, L. F., and Adanez, J., 1997, "Radial Gas Mixing in a Fast Fluidized Bed," Powder Technol., **94**(2), pp. 163–171.
[22] van Zoonen, D., 1962, "Measurements of Diffusional Phenomena and Velocity Profiles in a Vertical Riser," Symposium on Interaction Between Fluids and Particles, Institution of Chemical Engineers, London, pp. 64–71.
[23] Yang, G. L., Huang, Z., and Zhao, L., 1983, "Radial Gas Dispersion in a Fast Fluidized Bed," *Fluidization*, D. Kunii and R. Toei, eds., Cambridge University Press, Cambridge, UK, pp. 145–152.
[24] Werther, J., Hartge, E. U., and Kruse, M., 1992, "Gas Mixing and Interphase Mass Transfer in the Circulating Fluidized Bed," *Fluidization*, Vol. VII, O. E. Potter and D. J. Nicklin, eds., Engineering Foundation, New York, pp. 257–264.
[25] Amos, G., Rhodes, M. J., and Mineo, H., 1993, "Gas Mixing in Gas–Solids Risers," Chem. Eng. Sci., **48**(5), pp. 943–949.